Impact of Urban Expansion on Land Surface Temperature in Dodoma and Morogoro Metropolises, Tanzania

Sumari, N.S.[1,2], P.J. Mandela[2] and C.S. Swai[1,2]

[1]Department of Informatics and Information Technology, College of Natural and Applied Sciences (CoNAS), Sokoine University of Agriculture, Morogoro, Tanzania
[2]Centre for Earth Observation, Land and Geosciences Consultants (EOLGC), Aquila Eyes, Morogoro, Tanzania

*Corresponding author e-mail: *neydsumari@gmail.com*

Abstract

The study aims to evaluate the impact of metropolitan growth on land surface temperature (LST) in Dodoma and Morogoro metropolises. The paper adopts remote sensing methods to extract and analyze time-series Landsat satellite images from 2000 to 2018. An administered taxonomy was applied to map urban land-use change. Thermal and reflectance bands analysis were employed to retrieve and compare the Surface Temperature, Normalized Difference Vegetation Index (NDVI), urban expansion patterns, and the overall growth prominence in the cities. The results highlight a negative correlation between LST and NDVI, indicating that dissipating vegetation cover within the two study areas was responsible for the increase in LST over the study period. The outcome also showed that the metropolis of the study area rapidly expanded over the evaluation period with impermeable surface from 1.6% in 2000 to 5.3% in 2018 while non-impermeable decreased from 98.4% in 2000 to 94.7% in 2018. Increasing LST of annual-average of 31% in 2000 to 32% in 2018 was mostly due to conversion to the built-up area from non-built area. Therefore, the study concludes that LST is strongly influenced by land cover dynamics. The study suggests that planning of African cities should incorporate with sustainable and resilient urban future in order to improve the planning, compactness, sustainability and resilience of the urban environment.

Keywords: At-sensor brightness heat, urban planning, land surface temperature, SDGs, Dodoma, Morogoro

Introduction

There are many factors (natural and man-made) influencing land use and cover change, climate change and other physical and human environments. Perhaps, the most significant characteristics of man's induced changes on the environment are the variation recorded in thermal properties of the built, bare-land surfaces, soil and paved impervious surfaces which result in more solar energy being stored and converted to sensible heat, and also the removal of shrubs and trees which serve as a natural cooling effect of shading and evapotranspiration (Shao and Zhang, 2016; Sumari *et al.,* 2020; Wu *et al.,* 2021) and contribute to the reduction in outgoing longwave radiation by hindering the loss of sensible heat and distribution of heat (Ifatimehin, 2007; Ifatimehin *et al.,* 2009; Meng *et al.,* 2018).

For example, Feng (2019) and Meng *et al.,* (2018) reveal that the reduction of woodland and vegetation, which produce natural cooling from shading and evapotranspiration, are shown to contribute to the intensity of Land Surface Temperature (LST). LST is crucial to land surface processes particularly the transportation of temperature between the surface ground and an atmospheric boundary layer (Wang *et al.,* 2018; Zhang *et al.,* 2017), which can be recorded and estimated in the form of sensible heat fluctuation and latent heat fluctuation, or evapotranspiration (Bosco & Thomas, 2019; Li *et al.,* 2019; Peng *et al.,* 2017). In many cases, it has been established that human population concentration severely impacts LST as population density, a social variable, defines the scale and intensity of development within a defined location (Zhou *et al.,* 2019).

Studies show that urbanization has significant impact on micro and regional climate as the concentration of populations, industrial and economic activities transform the natural landscape to areas of largely built-up and paved surfaces, consequently impacting micro (city-level) and regional climate (Addaney and Cobbinah, 2019; Shao *et al.,* 2020). Some resultant effects of this altering micro and regional climate include extreme heat waves, and variable precipitation patterns with a higher risk of urban flooding or drought (Deilami *et al.,* 2018; Li *et al.,* 2018; Weng *et al.,* 2016). Globally, extreme heat waves are linked to increased heat-related mortalities and exacerbation of existing heath conditions such as respiratory and cerebral diseases (Analitis *et al.,* 2014; Lin *et al.,* 2009). While climate change and extreme heat waves resulting from LST are a global phenomenon, the impacts are not evenly distributed. Vulnerable and poorer regions such as Africa are heavily impacted due to poor land use planning, deficiency of basic infrastructure and services such as quality housing, water, and inefficient health care delivery system (Korah and Cobbinah, 2019). The ability to quantify urban growth and its relationship with LST distribution is crucial to developing sustainable and resilient communities and cities in line with achieving Sustainable Development Goal (SDG) 11. However, there is limited research examining spatio-temporal patterns and LST in African cities.

In situations of rapid and often unrecorded land use change, observations of the ground from space provide objective information and synoptic coverage of human consumption of the land. The application of remotely sensed data simplifies the synoptic analyses of earth observation, planning, and change at towns/cities, and regional scale over time (Cai *et al.,* 2017, Sumari *et al.,* 2017). Such data also provide an important link between intensive, localized ecological research and regional, national and international preservation and management of the environment (Cobbinah *et al.,* 2017; Korah *et al.,* 2017; Xu *et al.,* 2019a, 2019b). In addition, the synoptic coverage and accurate analysis presented by remote sensing (RS) data and Geospatial Information Science (GIS), respectively provides the basis for its adoption in estimating LST by several works (Hassaan *et al.,* 2019; Jeevalakshmi *et al.,* 2017; Peng *et al.,* 2017; Wijeratne *et al.,* 2018; Zhou *et al.,* 2019, 2014). Essentially, remote sensing is the main source for LST estimation at the regional and global scales (Wijeratne *et al.,* 2018) where as local level estimations may rely heavily on field data (Wang *et al.,* 2018).

Therefore, the main purpose of this research was to examine the rate of LST as influenced by changes in land cover in Dodoma City Council (DCC) and Morogoro Municipal Council (MMC). The specific goals of the study were to identify LST for the highest urban growth in the study areas, and to compare spatial and temporal variation of LST as a red-flagged indicator of unsustainable urban development in DCC and MMC, a situation that applies to most cities in sub-Saharan Africa. The study fills a useful knowledge gap for Tanzanian r as it aims at fulfilling a number of indicators for SDG 11 which collectively seek to "make cities and human settlements inclusive, safe, resilient and sustainable" by year 2030.

Materials and Methods
The Study Site

This study was conducted in Dodoma City Council (DCC) and Morogoro Municipal Council (MMC) as part of Dodoma and Morogoro regions, respectively, in Tanzania as shown in Figure 1. The geographical location of Dodoma region is in the central part of mainland Tanzania between latitude 40 and 70 South, and longitude 350 and 370 East. Administratively, the region is divided into seven districts as follows: Bahi, Chemba, Chamwino, DCC, Kondoa, Kongwe, and Mpwapwa (URT, 2010; URT, 2013). MMC is one of the nine districts in Morogoro Region. It is located between 370 East and 60 South of the Equator. Other districts include Kilosa, Ifakara, Kilombero, Malinyi, Mvomero, Gairo, Ulanga and Morogoro Rural.

The environment subtype of köppen climate taxonomy for Dodoma is "Bsh" or a mid-latitude steppe and desert climate. With an average annual temperature of 22.8°C, the warmest (19.40C) and coolest (19.40C) months are November and July, respectively. The average

annual precipitation in Dodoma is 563.9 mm, with an average of 42 days of rain (Weatherbase Dodoma, 2020). Meanwhile, the environment subtype of köppen climate taxonomy for Morogoro is "Aw" or a tropical savanna climate (Weatherbase Morogoro, 2020). The average annual temperature in Morogoro is 23.9°C with January as the warmest month (26.1°C), while July is the coolest month (21.1°C). The average annual precipitation in Morogoro is 889 mm, with an average of 60 days of rain annually.

October 2008, October 2016 and October 2018 for DCC of dry season to investigate the rate or urban temperature within each city. All Landsat images were gathered from the path/row number 168/064 and 167/065 for DCC and MMC (Table 1), respectively, with the same spatial resolution. Pre-processing such as radiometric and geometric correction were performed using ERDAS Imagine 2015 and ArcGIS 10.5. Seven land cover types (built-up, agriculture, water, woodland, bareland, wetland, and forest)
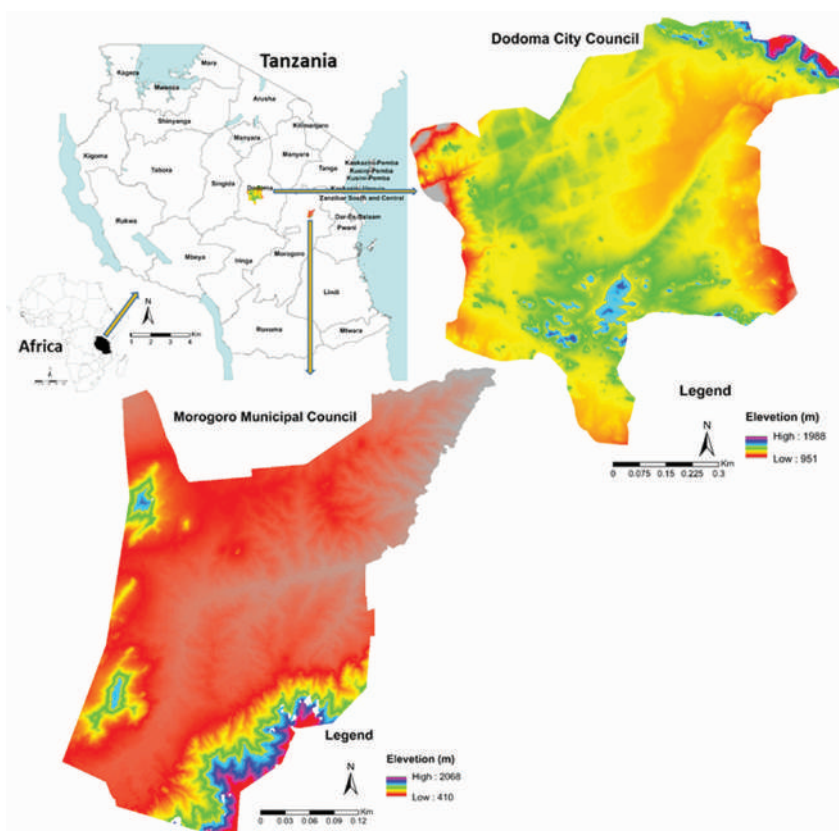

Figure 1: The study-setting showing, Dodoma City Council (DCC) and Morogoro Municipal Council (MCC)

Remote Sensing Data and Data processing

Cloud-free, Landsat 30m resolution satellite images were used to conduct urban heat study in DDC and MMC. Hence, the Landsat 30m products were obtained from http://earthexplorer.usgs.gov/ website of United States Geological Survey (USGS) for the years July 2000, September 2007, September 2017, and August 2018 for MCC and September 2000,

(NAFORMA, 2015) were identified through visual analysis and knowledge of the area. Random forest supervised image classification was used for image classification, which is most frequent and comprehensively been used in image classification methods in remote sensing (Shao *et al.,* 2016).

The classification accuracy assessment was implemented for each land cover type using

Table 1: Administrative Information of the study areas

Area	Location Path/Row	Land Area (Km²)	Wards	Estimated population 2002-2016	June-Oct (max & min temp)	Jul-Oct (mm) precipitation
DDC	168/064	2,576	37	326,811-454,128	31-18°C	0.03-2.08mm
MMC	167/065	540	28	227,921-359,684	35-24°C	17-25mm

training sampling points integrated with Google Earth Engine (satellite imagery) (Sumari *et al.,* 2020; Shelestov *et al.,* 2017). The result showed that the producer accuracy and user accuracy of all cities was higher than 87% (Fig. 11), which can achieve the correctness requirements for the land use change assessment.

$$L_\lambda = M_L Q_{cal} + A_L \qquad (1)$$

Where, L_λ indicates the Top-of-Atmospheric (TOA) spectral intensity $\left[\frac{Watts}{m^2 * Srad * \mu m}\right]$; M_L is band-precise multiplicative rescaling factor
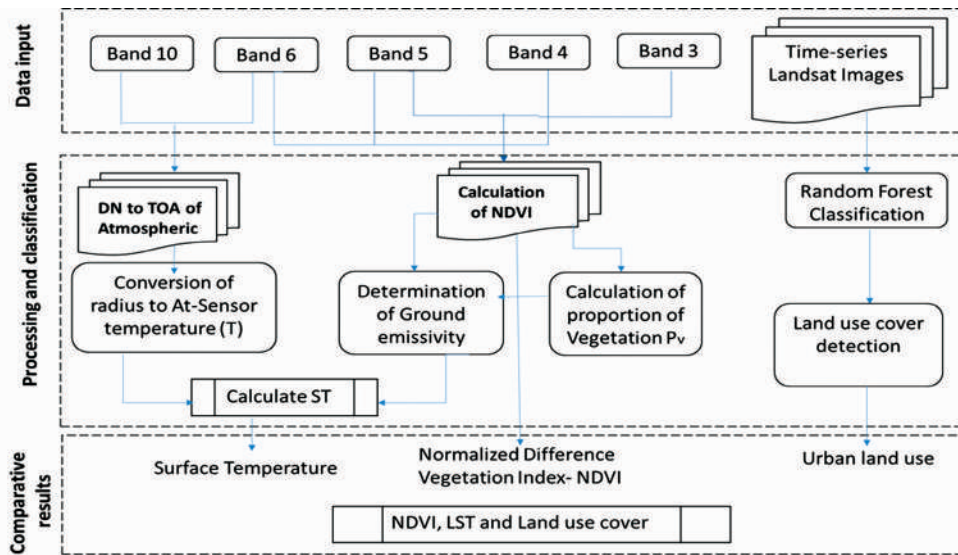

Figure 2: Workflow adopted for the study areas

Spatial-temporal dynamic of LST

The LST extraction approach used in the study is presented in Figure 2 above. Firstly, imagery is preprocessed using radiance scaling factors in statistic file then transformed to the digital number value of the pixels to the top-of-atmosphere (TOA) radiance through equation 1, and equation 2 to TOA reflectance values in equation 3, then conversion to At-Sensor brightness heat using equation 4. Finally, the LST, spatial patterns of land cover change were analyzed. The LST, Normalized Difference Vegetation Index (NDVI) and Normalized Difference Built Index (NDBI) were achieved using equations 5, 6 and 7.

from the statistical file, A_L is band-precise additive rescaling factor from the statistical file; Q_{cal} is Quantised and adjusted standard pixel value (DN).

$$P_\lambda = M_p Q_{cal} + A_p \qquad (2)$$

Where, P_λ represents the TOA without adjustment for solar angle; M_p is band-precise multiplicative rescaling factor from the statistic, A_p is band-precise extract rescaling factor from the statistic; Q_{cal} is Quantized and calibrated standard product pixel value (DN); were a rectification for the solar angle is qn. 3.

$$P_\lambda = \frac{P'_\lambda}{\cos\theta_{SZ}} = \frac{P'_\lambda}{\cos\theta_{SE}} \qquad (3)$$

Where, p_λ indicates TOA earthly reflectance; θ_{SZ} is local angle of sun elevation which is provided in the statistic file; θ_{ZE} is zenith angle;

Conversion to At-Sensor brightness heat, TIRS band data were transmuted from spectral radiant to intensity temperature using eq.4 thermal constants delivered in the statistic file.

$$T = \frac{K_2}{\ln\left(\frac{K_1}{L_\lambda}+1\right)} \tag{4}$$

Where, T represents the At-Sensor intensity heat (K); L_λ is TOA spectral brightness $\left[\frac{Watts}{m^2 * Srad * \mu m}\right]$; K_1 represent the constant

thermal conversion from the statistic file, K_1=666.09 and K_2=1282.71 for Landsat 7 (band 6) data while for Landsat 8 (band 10) K_1=774.88 and K_2=1321.08
Then we applied the equation 5 to calculate LST;

$$LST = BT / 1 + W * (BT/P) * \ln(e) \tag{5}$$

where: BT is At-Sensor brightness heat, W= wavelength of absorbed radiance (Landsat 8: band 10 and band 6); P=h*C⁄S (1.438*10⁻²) mk)=14380, Plank's constant h=6.626*10⁻³⁴) Js, Boltzmann constant S=1.38*10⁻²³)) J/K and

Velocity of bright C=2.998*10⁸ m/s. ln(e) is land cover from NDVI, where; e=0.004Pv+0.986 and Pv indicates the quantity proportion of the vegetation eq. 6

$$Pv = \left(\frac{NDVI_{max} - NDVI_{min}}{NDVI_{max} + NDVI_{min}}\right)^2 \tag{6}$$

Where: $NDVI_{max}$ is Normalized Difference Vegetation Index maximum for vegetation and $NDVI_{min}$ is Normalized Difference Vegetation Index minimum. Similarly, through eq. 7 we investigate green vegetation and crops patterns based on the reflectance,

$$NDVI = \left(Band_{NIR} - Band_{RED} / Band_{NIR} + Band_{NIR}\right) \tag{7}$$

Where: $Band_{NIR}$ (near-infrared) is surface reflectance of band 4 of TM/ETM plus, and $Band_{RED}$ is the surface reflectance of band 3 of TM/ETM plus images.

Results
Spatial pattern of the LULC in DCC and MMC

The spatial-temporal pattern of LULC of DCC and MMC from 2000 to 2018 (Fig. 3 and Fig. 4) indicates that there have been rapid land use and cover modification and alteration over the 18-year study period. The details for DCC show that while built-up and agricultural
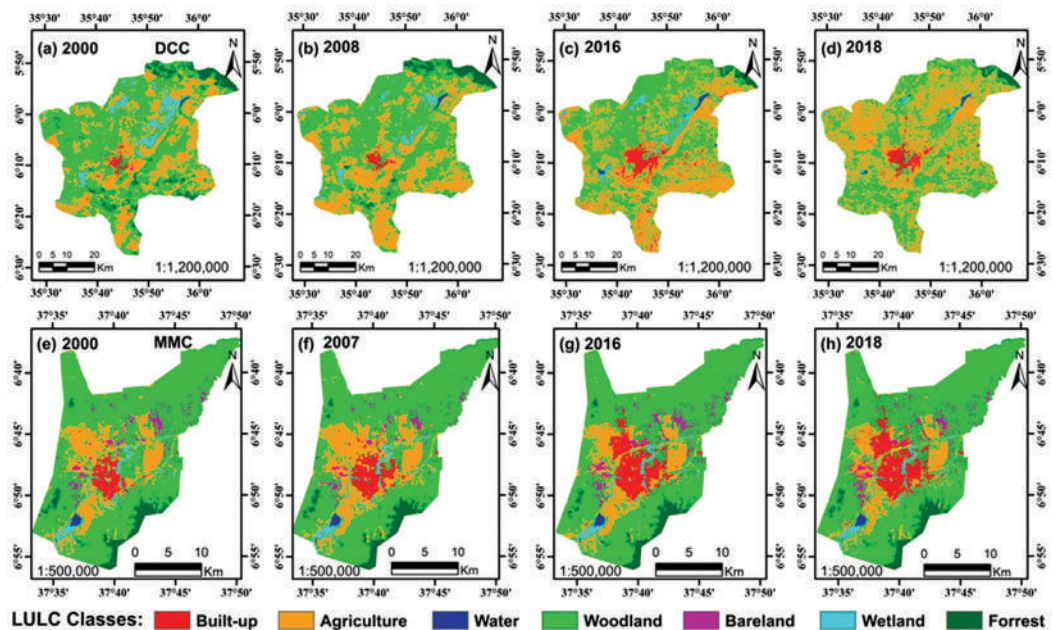

LULC Classes: ■ Built-up   ■ Agriculture   ■ Water   ■ Woodland   ■ Bareland   ■ Wetland   ■ Forrest

Figure 3: Spatial distribution of land cover map for Dodoma and Morogoro
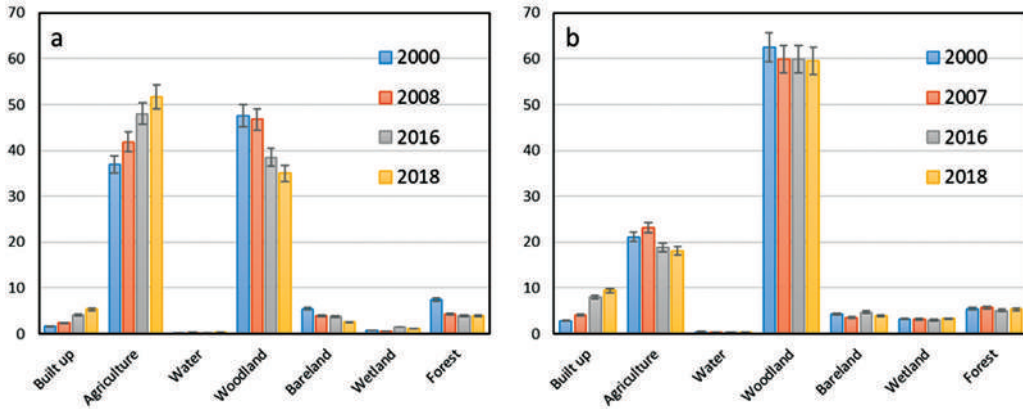
Figure 4: Rate of change for each LULC class in (a) DDC and (b) MMC

land increased (from 1.6% in 2000 to 5.3% in 2018 and from 37% in 2000 to 51% in 2018, respectively), woodland and forest land cover categories declined consistently (from 47.5% in 2000 to 33.5% in 2018 and from 7.5% in 2000 to 4.3% in 2018, respectively) over the study period. The greatest transformation for built-up land use (over 37 km^2) took place between the short periods of two years (2016 to 2018) while the entire land use, the woodland cover recorded the greatest decline (over 220 km^2) between 2008 and 2016. In the case of MMC, the built-up category is by far the most expansive land cover type over the 18-year study period with a total expansion area of over 34 km^2. Over the same period, agricultural land declined by almost 17 km^2. Comparatively, the land use and cover of DCC recorded a more drastic transformation than that of the MMC.

Urban Expansion, Population Growth in DCC & MMC

The metropolitan mark (Fig. 5 and Table 2) shows that much of the metropolitan development took place northward of both cities. For DCC, the ultimate urban expansion was recorded from 2016 to 2018 and from 2008 to 2016 converting an area of 38 km^2 and 40 km^2, respectively. This pattern is correlated with population increase (Fig. 6) detailed during the same period where the MMC recorded an increase in population from about 190,000 in the year 2000 to over 310,000 in 2017, while DCC recorded a population increase from about
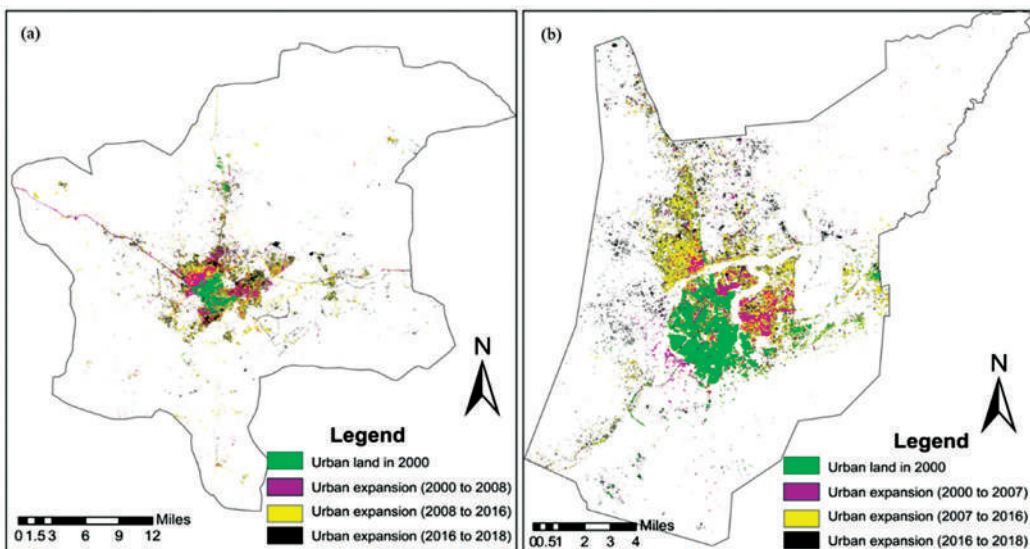

Figure 5: Urban footprint of (a) DCC and (b) MMC from 2000 to 2018

Table 2: Urban land (Km²) and proportion (%) of the urban expansion from 2000 to 2018

City	Urban Land Area (Km²)				Urban Land Expansion (%)			
DCC	2000	2008	2016	2018	2000-2008	2008-2016	2016-2018	2000-2018
	43	62	102	140	0.7	1.6	1.4	3.7
MCC	2000	2007	2016	2018	2000-2007	2007-2016	2016-2018	2000-2018
	15.5	21.9	43.3	51.1	1.2	3.9	1.5	6.6

310,000 in the year 2000 to 450,000 in 2017. A very high variance dependency (0.9994 and 0.9996 for DCC and MMC, correspondingly) is established between population growth, as an independent variable, and urban expansion, as a dependent variable (Fig. 6). Moreover, the correlation between urban development (roads, buildings, impervious surfaces, etc.) and increased heat island or surface temperature have been established by several studies including Yang *et al.,* (2019) and Zhou *et al.,* (2019).

indication of healthy vegetation) than degraded areas. Relatively, the. maximum NDVI values were recorded in MMC. In general, extraction of NDVI pixels for our region of interest (ROI) provides values that range from a low of -0.17 to a maximum of 0.77 for DCC and a low of -0.18 to a maximum of 0.97 for MMC. According to Cao *et al.* (2018), NDVI values of +1 (0.8 - 0.9) signify dense forests, >0.3-0.5 represents medium vegetation and >0.1 to 0.3 represents low vegetationThe applicability of NDVI in this study is thought to be relevant for the reason that
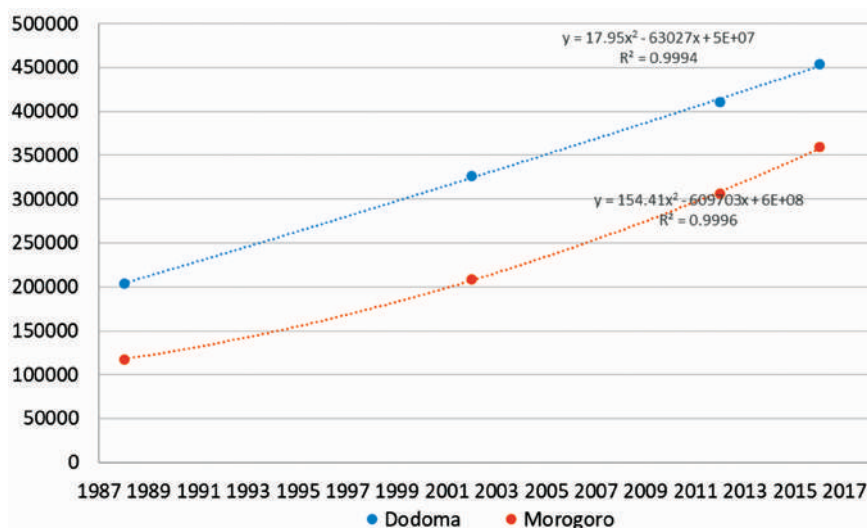

Figure showing population growth trend with equations $y = 17.95x^2 - 63027x + 5E+07$, $R^2 = 0.9994$ and $y = 154.41x^2 - 609703x + 6E+08$, $R^2 = 0.9996$

Figure 6: Population growth trend for DCC and MCC

The Estimation of NDVI and spatial distribution of LST

The NDVI indices and LST have been mapped across the two metropolitan centers (Fig. 7 & 8). NDVI have been improved and taken up to the experimental amount of urban land. Assessments of vegetation in the study area were performed as a step towards the fortitude of the vegetation health over the period of eighteen years' time-period. Figure 7 shows that the healthy and non-degraded component of the study area discovered high NDVI (an

the amount and quality of vegetation present within the MMC and DCC are significant factors, and can be used to infer general vegetation situation which in turn serve as an inferential basis for moisture content levels of soils (Ujoh *et al.* 2019; Xiong *et al.* 2017). The NDVI maps show a constantly and sequentially a slighter difference between the near-infrared and the red reflectance, hence implying smaller vegetation index over the study years (from 2000 to 2018) for both locations.
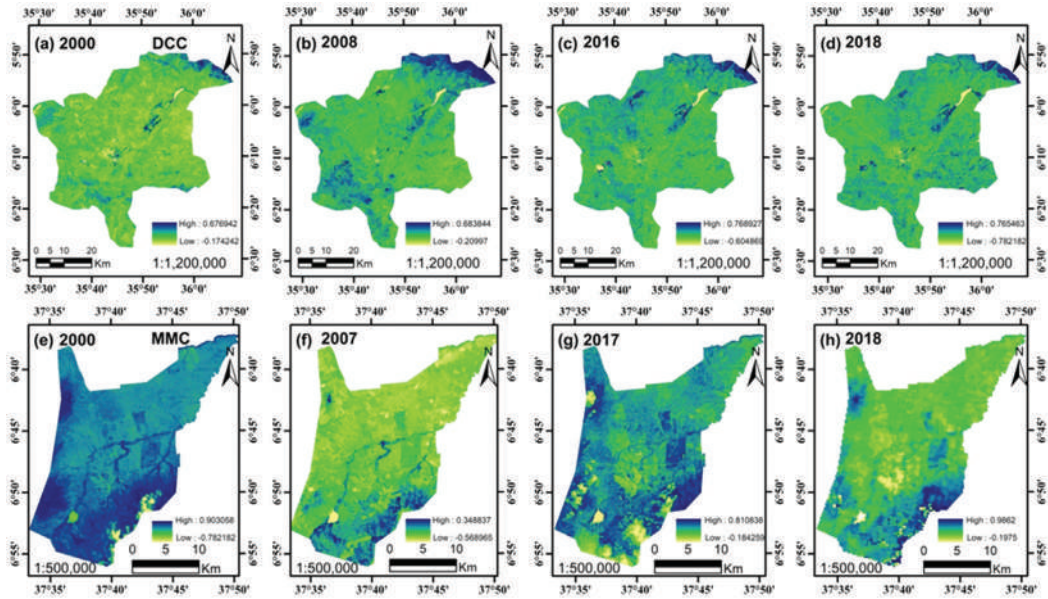
Figure 7: Spatial distributions of the NDVI of DCC (a, b, c, d) and MMC (e, f, g, h)

The LST maps (Fig. 8) reveal minimum and maximum temperatures of 6°C and 54°C in DDC and MMC with a high proportion of temperature levels ranging from around 28°C to 35°C. The industrial land cover taken on for this study refers to the overall metropolitan surface land cover, which includes concrete and corrugated building roofs, streets, and other pervious and impervious surfaces within the two metropolitan centers. The results show that the built-up land cover has time after time extended from 1.6% in 2000 to 5.3% in 2018, in tandem with surface temperature increase within the same period.

In examining the different dynamics, which interplay in increasing the LST in some cities, a major focus was given to urban environmental components (such as NDVI, land-use, and population density) that determine temperature variation. Although, the study considered land-use changes in the urban area as the major factor driving LST, results of analyses of satellite images in Dodoma show higher LST values
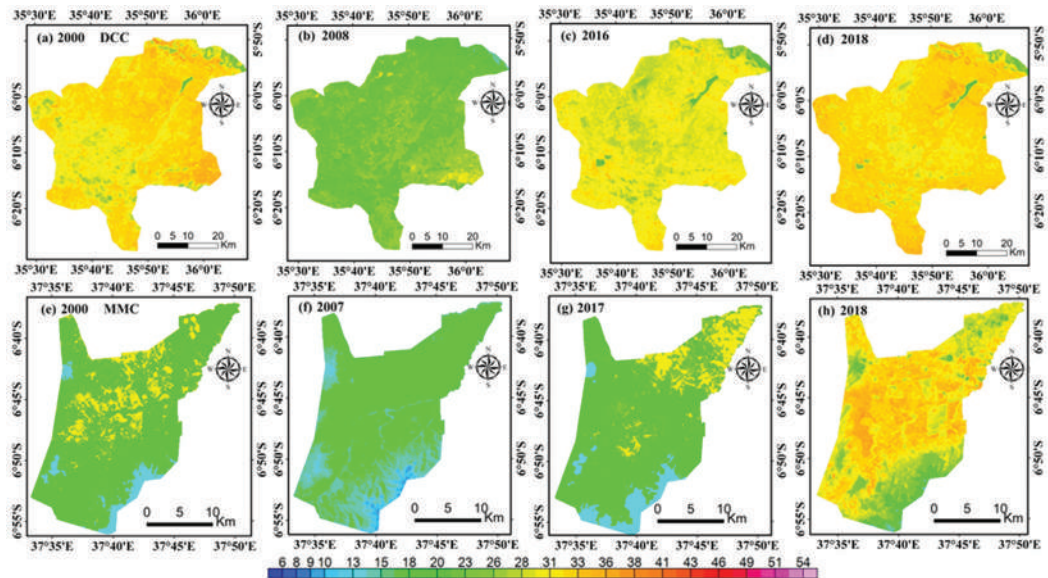

Figure 8: Spatial distributions of the LST of DCC (a, b, c, d) and MMC (e, f, g, h)

in 2018 than 2000, while both urban areas have more built-up in the year 2018 than 2000. According to Table 2, land-use change pattern of those areas were distressed by the increase of LST value in 2018.
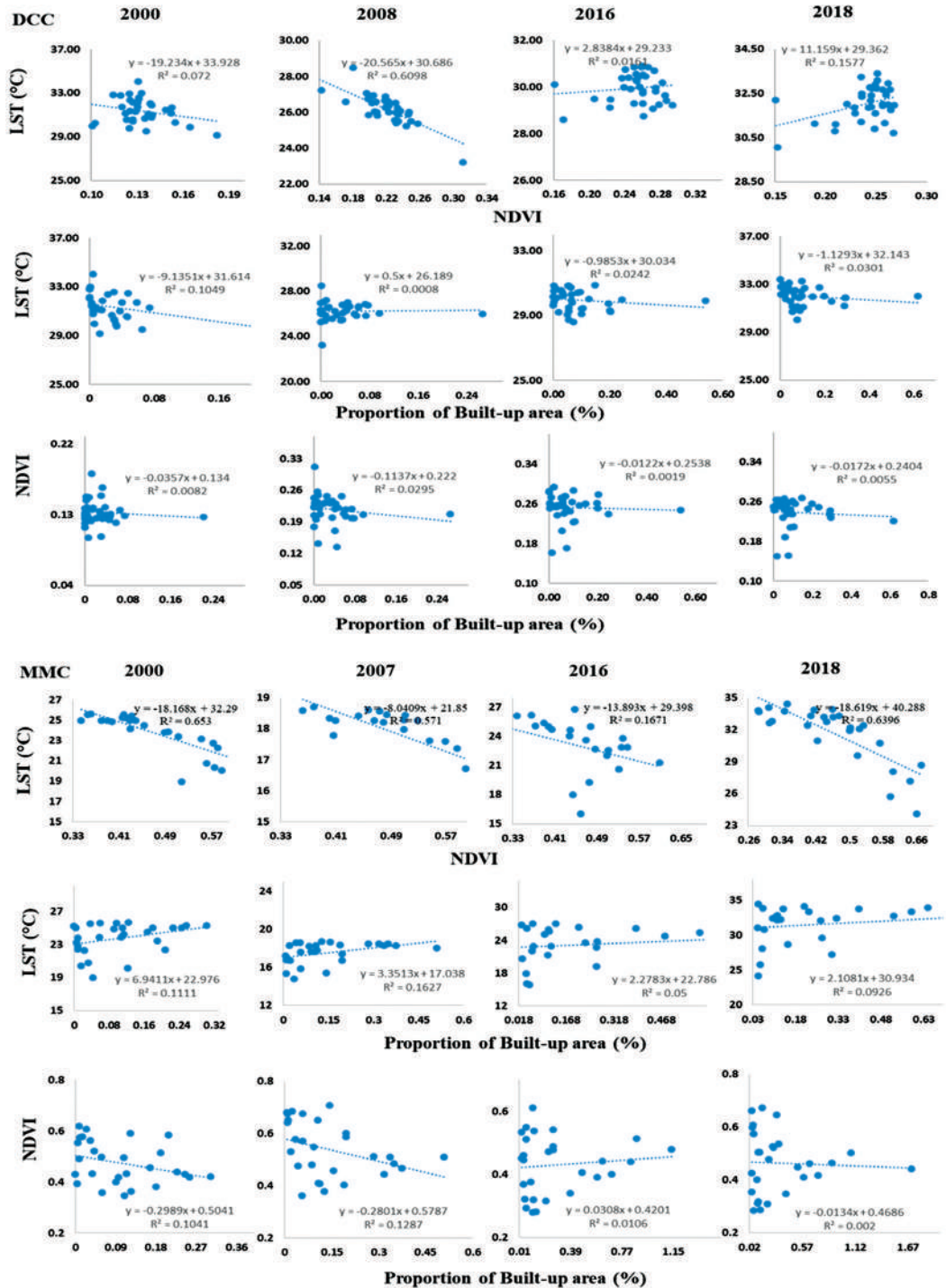

Figure 9: The correlation coefficient of the average LST, the NDVI and the built up percentages for DCC and MMC

Correlation Coefficient of NDVI, LST and Built-up for DCC and MMC

The correlation coefficient is used in this study to calculate the strength and direction of the relationship between LST and NDVI, LST and built-up area, and NDVI and built-up area for DCC and MMC. The results (presented as Fig. 9) show that the strength of relationship between NDVI and LST for year 2008 in DCC is relatively stronger negative (at -0.061) implying that the two variables are strongly correlated in opposite directions. In essence, as the value of NDVI increases, that of LST decreases and vice versa. The correlation coefficient results for LST and built-up area, and NDVI and built-

$(R^2=0.57)$ and 2018 $(R^2=0.64)$. However, for the correlation between LST and built-up proportion, the strength of the relationship is positively weak, meaning that although the relationship is statistically insignificant in terms of strength, an increase in LST means there is an increase in built-up area and vice versa. Similarly, the relationship between NDVI and built-up land cover for MMC is a negative one, in spite of its statistical insignificance of the producers and user's accuracy assessment of classified Landsat images that are statistically significant and acceptable for further analysis by urban planners and environmental experts (Fig. 10).
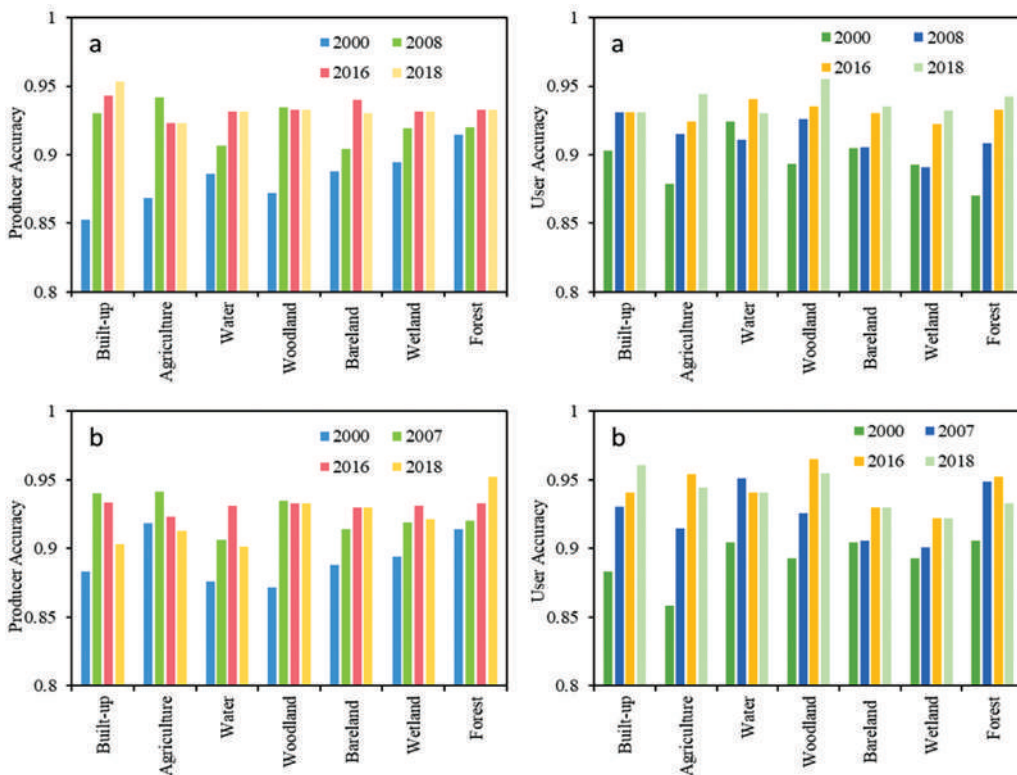

Figure 10: The percentage of accuracy assessment for each classified classes in (a) DCC and (b) MMC

up area for DCC show statistically insignificant results. For MMC, the results of the regression of correlation analysis between LST and NDVI from 2000 to 2018 as dependent variable (N=number of Wards), exhibits a strong positive relationship for the years 2000 $(R^2=0.65)$, 2007

Discussion

Urban expansion is one of the most significant components of global change responsible for modification of the land-use surface, species diversity, and quality of human life (Lourenço *et al.,* 2018). It is expected that

an improved knowledge of urban expansion and global heat will contribute to emerging a more sustainable environment for rapidly expanding urban areas. Using Multi-temporal Landsat TM/ETM+ imagery, land use change detection techniques were applied to quantify urban expansion patterns as well as its impacts on Land Surface Temperature (LST). Rapid increase of built-up area from 2000 to 2018 in DCC and MMC was determined. The percentage of urban expansion from 2000-2008, 2008-2016, 2016-2018 for DCC was 0.7, 1.6, 1.4, 3.7%, respectively, and from 2000-2007, 2007-2016, 2016-2018, MCC increased by 1.2%, 3.9%, 1.5%, 6.6%, respectively. The impact of urban expansion was the decrease of agriculture land, woodland and forest area in both two cities. For example, Sumari *et al.,* (2019) shows that in Morogoro urban the most significant land use change was the conversion from farmland to built-up area. Urban expansion which arisen mostly around the midpoint of the city (city center) was associated with population growth and economic development. Essentially, the population of Morogoro Municipal was 227,921 and 359,684 thousand while in Dodoma City Council was 236,811 and 454,128 from 2002 and 2016. Rapidly increasing population prompted the expansion of urban land cover and the conversion of agricultural land and forest to impermeable surface. Therefore, these impermeable surfaces have relatively higher LST, which may lead to temperature increase in the long run. (Weng *et al.,* 2019; Weng and Fu, 2014; Zhou *et al.,* 2014)

Given the rate of expansion of Morogoro and Dodoma urban areas triggered by the increasing urban population, there is a corresponding intensity in demand for resources including energy, water and land which collectively heightens the need to improve urban management and planning for sustainability (Gao *et al.,* 2015). For example, it is becoming increasing necessary for cities to adopt smart and sustainable approaches through the usage of renewable energy sources rather than remnant fuel powered energy sources that cause pollution. More specifically, urban planning strategies need to account for different consequences that address urban growth patterns and reverses declining/worsening micro-climatic conditions.

Conclusion

This study has investigated the outcome of urban expansion on the land surface temperature of Dodoma and Morogoro urban areas with a number of observations gathered from the study. Firstly, both towns have experienced rapid growth due to increase in population between the periods 2000 to 2018. Secondly, there has been remarkable degradation of vegetation land cover areas in favour of increased built-up areas. The outcome shows that, the land surface temperature of Morogoro municipal and Dodoma city were amplified through the study period with a high LST of (>23°C). The results also show that NDVI and LST present a negative correlation, while built-up areas and LST reveal positive correlation, which confirms that the densely built-up and residential areas have recorded high increase in LST. To address these challenges, it is pertinent that future urban city designs and planning should incorporate greening. Finally, the study revealed that the rising population growth and urban expansion directly affect the increase in built-up areas, which consequently lead to an increase in LST.

References

Addaney, M., and Cobbinah, P.B. (2019). Climate Change, Urban Planning and Sustainable Development in Africa: The Difference Worth Appreciating. In The Geography of Climate Change Adaptation in Urban Africa. Springer International Publishing. https://doi.org/10.1007/978-3-030-04873-0_1

Bosco, N.J., & Thomas, M. (2019). Land Surface Temperature Analysis of Kigali City. *Current Journal of Applied Science and Technology,* 32(2), 1–11. https://doi.org/10.9734/cjast/2019/45426

Cai, Y., Chen, G., Wang, Y., & Yang, L. (2017). Impacts of land cover and seasonal variation on maximum air temperature estimation using MODIS imagery. Remote Sensing, 9(3). https://doi.org/10.3390/rs9030233

Cao, R., Chen, Y., Shen, M., Chen, J., Zhou, J., Wang, C., & Yang, W. (2018). A simple method to improve the quality of NDVI time-

series data by integrating spatiotemporal information with the Savitzky-Golay filter. Remote Sensing of Environment, 217(December 2017), 244–257. https://doi.org/10.1016/j.rse.2018.08.022

Cobbinah, P.B., Poku-Boansi, M., & Peprah, C. (2017). Urban environmental problems in Ghana. Environmental Development, 23(December 2016), 33–46. https://doi.org/10.1016/j.envdev.2017.05.001

Deilami, K., Kamruzzaman, M., & Liu, Y. (2018). Urban heat island effect: A systematic review of spatio-temporal factors, data, methods, and mitigation measures. International Journal of Applied Earth Observation and Geoinformation, 67(January), 30–42. https://doi.org/10.1016/j.jag.2017.12.009

Gao, B., Huang, Q., He, C., & Ma, Q. (2015). Dynamics of urbanization levels in China from 1992 to 2012: Perspective from DMSP/OLS nighttime light data. Remote Sensing, 7(2), 1721–1735. https://doi.org/10.3390/rs70201721

Hassaan, A.M., Belal, A.A., Hassan, M.A., Farag, F.M., & Mohamed, E.S. (2019). Potential of thermal remote sensing techniques in monitoring waterlogged area based on surface soil moisture retrieval. *Journal of African Earth Sciences,* 155, 64–74. https://doi.org/10.1016/j.jafrearsci.2019.04.005

Jeevalakshmi, D., Narayana Reddy, S., & Manikiam, B. (2017). Land surface temperature retrieval from LANDSAT data using emissivity estimation. *International Journal of Applied Engineering Research,* 12(20), 9679–9687.

Korah, P.I., Cobbinah, P.B., & Nunbogu, A.M. (2017). Spatial planning in Ghana: Exploring the contradictions. Planning Practice and Research, 32(4), 361–384. https://doi.org/10.1080/02697459.2017.1378977

Li, G., Lu, D., Moran, E., Calvi, M.F., Dutra, L. V., & Batistella, M. (2019). Examining deforestation and agropasture dynamics along the Brazilian TransAmazon Highway using multitemporal Landsat imagery. GIScience and Remote Sensing, 56(2), 161–183. https://doi.org/10.1080/1548160 3.2018.1497438

Li, Z., Wang, C., Emrich, C.T., & Guo, D. (2018). A novel approach to leveraging social media for rapid flood mapping: a case study of the 2015 South Carolina floods. Cartography and Geographic Information Science, 45(2), 97–110. https://doi.org/10.1080/15230406.2016.1271356

Lourenço, P., Alcaraz-Segura, D., Reyes-Díez, A., Requena-Mullor, J.M., & Cabello, J. (2018). Trends in vegetation greenness dynamics in protected areas across borders: what are the environmental controls? *International Journal of Remote Sensing,* 39(14), 4699–4713. https://doi.org/10.1080/01431161.2018.1466080

Peng, W., Zhou, J., Wen, L., Xue, S., & Dong, L. (2017). Land surface temperature and its impact factors in Western Sichuan Plateau, China. Geocarto International, 32(8), 919–934. https://doi.org/10.1080/10106049.2016.1188167

Shao, Z., Fu, H., Fu, P., & Yin, L. (2016). Mapping urban impervious surface by fusing optical and SAR data at the decision level. Remote Sensing, 8(11). https://doi.org/10.3390/rs8110945

Shao, Z., Fu, H., Li, D., Altan, O., & Cheng, T. (2019). Remote sensing monitoring of multi-scale watersheds impermeability for urban hydrological evaluation. Remote Sensing of Environment, 232(October 2018), 111338. https://doi.org/10.1016/j.rse.2019.111338

Shao, Z., & Zhang, L. (2016). Estimating forest aboveground biomass by combining optical and SAR data: A case study in genhe, inner Mongolia, China. Sensors (Switzerland), 16(6). https://doi.org/10.3390/s16060834

Shelestov, A., Lavreniuk, M., Kussul, N., Novikov, A., & Skakun, S. (2017). Large scale crop classification using Google earth engine platform. International Geoscience and Remote Sensing Symposium (IGARSS), 2017-July, 3696–3699. https://doi.org/10.1109/IGARSS.2017.8127801

Silva, P., & Li, L. (2017). Mapping urban expansion and exploring its driving forces in the city of Praia, Cape Verde, from 1969 to 2015. Sustainability (Switzerland), 9(8),

1434. https://doi.org/10.3390/su9081434

Sumari, N.S., Cobbinah, P.B., Ujoh, F., & Xu, G. (2020). On the absurdity of rapid urbanization: Spatio-temporal analysis of land-use changes in Morogoro, Tanzania. Cities, 107(June), 102876. https://doi.org/10.1016/j.cities.2020.102876

Sumari, N.S., Xu, G., Ujoh, F., Korah, P.I., Ebohon, O.J., & Lyimo, N.N. (2019). A geospatial approach to sustainable urban planning: Lessons for Morogoro Municipal Council, Tanzania. Sustainability (Switzerland), 11(22), 1–14. https://doi.org/10.3390/su11226508

Tanzania Forest Service Agency. (2015). National Forest Resources Monitoring and Assessment of Tanzania Mainland (Issue May). http://naforma.mnrt.go.tz

Terfa, B.K., Chen, N., Liu, D., Zhang, X., & Niyogi, D. (2019). Urban expansion in Ethiopia from 1987 to 2017: Characteristics, spatial patterns, and driving forces. Sustainability (Switzerland), 11(10). https://doi.org/10.3390/su11102973

Ujoh, F., Kwabe, I., Ifatimehin, O.O., & D,I. (2010). Understanding urban sprawl in the Federal Capital City, Abuja: Towards sustainable urbanization in Nigeria. *Journal of Geography and Regional Planning,* 3(5), 106–113.

Wang, S., Ma, Q., Ding, H., & Liang, H. (2018). Detection of urban expansion and land surface temperature change using multi-temporal landsat images. Resources, Conservation and Recycling, 128, 526–534. https://doi.org/10.1016/j.resconrec.2016.05.011

Weng, Q., Firozjaei, M.K., Sedighi, A., Kiavarz, M., & Alavipanah, S.K. (2019). Statistical analysis of surface urban heat island intensity variations: A case study of Babol city, Iran. GIScience and Remote Sensing, 56(4), 576–604. https://doi.org/10.1080/15481603.2018.1548080

Weng, Q., & Fu, P. (2014). Modeling annual parameters of clear-sky land surface temperature variations and evaluating the impact of cloud cover using time series of Landsat TIR data. Remote Sensing of Environment, 140, 267–278. https://doi.org/10.1016/j.rse.2013.09.002

Weng, Q., Hua nan shi fan da xue, IEEE Geoscience and Remote Sensing Society, & Institute of Electrical and Electronics Engineers. (2016). Proceedings of EORSA 2016: the Fourth International Workshop on Earth Observation and Remote Sensing Applications (EORSA 2016). 2016 Fourth International Workshop on Earth Observation and Remote Sensing Applications.

Wijeratne, V.P.I.S., Manawadu, L., & Ranasinghe, P. (2018). A Study of Land Surface Temperature Variation in Selected Urban Cities in Sri Lanka. *International Journal of Scientific and Research Publications* (IJSRP), 8(10). https://doi.org/10.29322/ijsrp.8.10.2018.p8251

Wu, S., Sumari, N.S., Dong, T., Xu, G., & Liu, Y. (2021). Characterizing Urban Expansion Combining Concentric-Ring and Grid-Based Analysis for Latin American Cities. Land. https://doi.org/https://doi.org/10.3390/land10050444

Xiong, J., Thenkabail, P.S., Gumma, M.K., Teluguntla, P., Poehnelt, J., Congalton, R.G., Yadav, K., & Thau, D. (2017). Automated cropland mapping of continental Africa using Google Earth Engine cloud computing. *ISPRS Journal of Photogrammetry and Remote Sensing,* 126: 225–244. https://doi.org/10.1016/j.isprsjprs.2017.01.019

Xu, G., Jiao, L., Liu, J., Shi, Z., Zeng, C., & Liu, Y. (2019). Understanding urban expansion combining macro patterns and micro dynamics in three Southeast Asian megacities. Science of the Total Environment, 660(41771429), 375–383. https://doi.org/10.1016/j.scitotenv.2019.01.039

Zhang, L., Weng, Q., & Shao, Z. (2017). An evaluation of monthly impervious surface dynamics by fusing Landsat and MODIS time series in the Pearl River Delta, China, from 2000 to 2015. Remote Sensing of Environment, 201(August), 99–114. https://doi.org/10.1016/j.rse.2017.08.036

Zhou, D., Xiao, J., Bonafoni, S., Berger, C., Deilami, K., Zhou, Y., Frolking, S., Yao,

R., Qiao, Z., & Sobrino, J.A. (2019). Satellite remote sensing of surface urban heat islands: Progress, challenges, and perspectives. Remote Sensing, 11(1), 1–36. https://doi.org/10.3390/rs11010048

Zhou, D., Zhao, S., Liu, S., Zhang, L., & Zhu, C. (2014). Surface urban heat island in China's 32 major cities: Spatial patterns and drivers. Remote Sensing of Environment, 152, 51–61. https://doi.org/10.1016/j.rse.2014.05.017.